Materials Horizons

Stress-Localized Durable Icephobic Surfaces

Journal:	*Materials Horizons*
Manuscript ID	MH-COM-10-2018-001291.R2
Article Type:	Communication
Date Submitted by the Author:	14-Dec-2018
Complete List of Authors:	Irajizad, Peyman; University of Houston System, Mechanical Engineering Al-Bayati, Abdullah ; University of Houston System, Mechanical Engineering Eslami, Bahareh; University of houston, Mechanical Engineering Shafquat, Taha ; University of Houston System, Mechanical Engineering Nazari, Masoumeh; University of Houston Jafari, Parham; University of Houston, Mechanical Engineering Kashyap, Varun ; University of Houston System, Mechanical Engineering Masoudi, Ali; University of Houston System, Department of Mechanical Engineering Araya, Daniel ; University of houston, Mechanical Engineering Ghasemi, Hadi; University of Houston System, Mechanical Engineering

Conceptual Insights Statement

We developed underlying physics of stress-localization concept to minimize adhesion of a solid on a surface. The fundamental underpinnings of this concept are elucidated and a simple formulation is derived that could be used to characterize solid adhesion on various surfaces. Through this concept, we developed a new icephobic material system with ice adhesion of an order of magnitude lower than state-of-the-art materials while having long-term mechanical, chemical and environmental durability. As demonstrated, concept of stress-localization is far more effective than previously studied surface-modified methods (e.g. perfluorinated or hydrated surface). Stress-localization is a volumetric phenomenon and remains effective even after long duration of operation of these materials. The general concept of stress-localization could be implemented in a broad range of material systems to minimize adhesion of any solid including bio-species, salt, dust and gas hydrates on surfaces with a wide range of application from aviation systems, oceanic sciences, energy systems to bio-sciences.

Materials Horizons

COMMUNICATION

Stress-Localized Durable Icephobic Surfaces

Peyman Irajizad[a], Abdullah Al-Bayati[a], Bahareh Eslami[a], Taha Shafquat[a], Masoumeh Nazari[a], Parham Jafari[a], Varun Kashyap[a], Ali Masoudi[a], Daniel Araya[a,b] and Hadi Ghasemi[a*]

Received 00th January 20xx,
Accepted 00th January 20xx

DOI: 10.1039/x0xx00000x

www.rsc.org/

Icephobic surfaces have a critical footprint on human daily lives in cold climates ranging from aviation systems and infrastructures to energy systems. However, creation of these surfaces for low-temperature applications remains elusive. Non-wetting, liquid-infused and hydrated surfaces have inspired routes for development of icephobic surfaces. However, high ice adhesion strength (~20-100 kPa) and subsequent ice accretion, low long-term mechanical and environmental durability, and high production cost have restricted their applications. Here, we cast fundamentals of a new physical concept called stress-localization to develop icephobic surfaces with ice adhesion in order of 1 kPa and exceptional mechanical, chemical and environmental durability.

Conceptual insight

We developed underlying physics of stress-localization concept to minimize adhesion of a solid on a surface. The fundamental underpinnings of this concept are elucidated and a simple formulation is derived that could be used to characterize solid adhesion on various surfaces. Through this concept, we developed a new icephobic material system with ice adhesion of an order of magnitude lower than state-of-the-art materials while having long-term mechanical, chemical and environmental durability. As demonstrated, concept of stress-localization is far more effective than previously studied surface-modified methods (e.g. perfluorinated or hydrated surface). Stress-localization is a volumetric phenomenon and remains effective even after long duration of operation of these materials. The concept of stress-localization could be implemented in a broad range of material systems to minimize adhesion of any solid including bio-species, salt, dust and gas hydrates on surfaces with a wide range of application from aviation systems, oceanic sciences, energy systems to bio-sciences.

Introduction

Icing is an omnipresent phenomenon in nature[1,2] and technology[3], and impacts a broad spectrum of industries ranging from transportation systems[4–6], power transmission lines[7], and infrastructures[8,9] to energy systems[10]. Icing in aircrafts results in increased drag and may lead to loss of lift force and potential catastrophic events. Icing in electricity transmission systems can lead to collapse of poles and towers and rupture of conductors. Icing in cooling systems significantly drops the heat transfer rate leading to their inefficient operation. Although anti-icing surfaces play a vital role in society, development of durable and high-performance surfaces for such demanding applications remains elusive. According to Congressional Research Report, ice storms account for 5% of power transmission outages in US[11]. As a result, the financial loss for such industries is approximated between $5-8 billion annually. Additionally, around three million people in the US, suffer every winter from power losses caused by ice storms[12]. Icephobicity is the ability of a surface to minimize ice adhesion and accretion onto a surface. Two main figures of merit for icephobic surfaces are adhesion strength at the ice-solid interface, and long-term durability when exposed to severe mechanical, chemical and environmental conditions. Specifically, for aerospace applications, long-term durability under high shear flows, durability under erosive conditions including sand and rain, durability under UV exposure, aerodynamics characteristics, and quick field repairability are of critical importance.

A range of surfaces (e.g. superhydrohobic, liquid-infused and hydrated surfaces) has been developed to address the icing challenge. However, the developed surfaces have either shown incremental improvements in performance or have not satisfied the required figures of merit. Early in development of anti-icing surfaces, Superhydrophobic surfaces were developed through micro/nano structuring on hydrophobic surfaces[13–19] (or hydrophilic surfaces)[20,21]. Although the droplet contact area on superhydrophobic surfaces is reduced[22,23], the micro/nano structuring of surface and frost formation in these structures affects ice adhesion strength. The reported ice adhesion on superhydrophobic surfaces is in the range of 100-500 kPa, which is of similar magnitude to adhesion strengths measured on smooth metal surfaces (~100 kPa) [19,24,25]. Recently,

[a] Department of Mechanical Engineering, University of Houston, Houston, TX 77204-4006, USA
[b] Johns Hopkins University Applied Physics Laboratory
† Correspondence to: hghasemi@uh.edu.
Electronic Supplementary Information (ESI) available: [Standard method of adhesion measurement, details of mathematical derivations, material synthesis, and experimental setups]. See DOI: 10.1039/x0xx00000x

Materials Horizons

COMMUNICATION

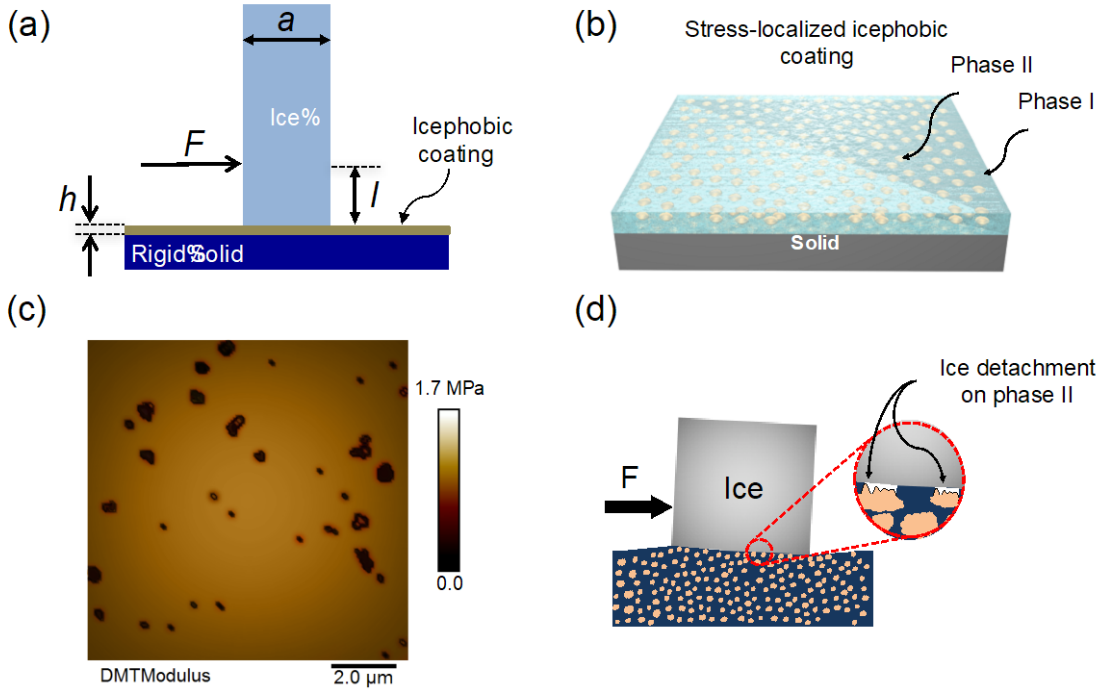

Figure 1. (a) Schematic of ice detachment from the icephobic material, (b) stress-localized icephobic surfaces, (c) Surface map of elastic modulus of stress-localized materials, (d) formation of crack at the coordinate of phase II with minimal forces.

slippery liquid infused porous surfaces (SLIPS) have been created, which utilize the smooth nature of liquid surface to improve icephobicity[26]. This smooth surface mitigates pinning of water droplets on these surfaces[27] and reduce ice adhesion strength[28] to values between 10 and 150 kPa. However, after few cycles of icing-deicing, the liquid layer depletes and the ice adhesion increases to the order of 200 kPa [29]. One of the interesting features of ice is the existence of a thin liquid-like transition layer at the surface even at freezing temperatures, which makes ice slippery[30–34]. This thin film makes it possible to skate at freezing temperatures. This feature has been exploited in development of hydrated icephobic surfaces that promote formation of aqueous lubricating layer with no need for additional oil. While the lubricating film exists on the surface (i.e. in the temperature range of 0 to -25 °C), ice adhesion on these surfaces is in the range of 20-60 kPa[35–37]. However, at lower temperatures, the change in molecular configuration of the transition film drastically boosts the ice adhesion to values in the order of 1000 kPa [35]. The idea of a non-frozen liquid-like layer at the ice surface inspired Chen et al.[38] to develop a new type of icephobic material that keeps a quasi-liquid layer on its surface and shows ice adhesion strength of 50 kPa. With another approach, Golovin et al.[39] exploited modified elastomers to reduce ice adhesion. In this approach, the shear modulus of various elastomers was reduced by reducing the cross-linking density of the structure and interfacial slippage was activated at the interface by embedding miscible polymeric chains. The authors reported that the stress required for *motion* of ice on the surface is in the range of 0.2-10 kPa. However, the stress required for motion of ice on a surface is different from the adhesion strength. While in the former case, ice is still in contact with the surface, in the latter case the induced stress detaches ice from the surface. The adhesion stress is the critical stress (maximum stress) at which ice detaches from the surface. Furthermore, the adhesion stress on elastomers is a function of shear rate and can vary by an order of magnitude depending on the applied shear rate. Thus, to compare these reported values of ice adhesion with the other reported values, a standard test protocol needs to be followed. Due to absence of this standard protocol, the reported values of ice adhesion for PDMS varies in the range of 100-800 kPa[24,40,41]. In another approach, Zhiwei et al.[42] used pre-developed micro-holes in the PDMS structure to help on formation of cracks at the interface and reduce ice adhesion. These pre-developed holes are made through micro/nano fabrication. They used idea of stiffness inhomogeneity to reduce ice adhesion. Through this approach, the authors could reduce ice adhesion by ~ 50%. Recently, Irajizad et al.[43–45] introduced the concept of magnetic slippery surfaces (MAGSS) by exploiting magnetic force to induce a liquid-liquid interface. These surfaces show extreme icephobicity with ice adhesion of 2 Pa. However, the liquid nature of these surfaces limits their mechanical durability in long-term performance.

Here, we have developed a new physical concept and the corresponding icephobic material that shows extremely low ice adhesion while having long-term mechanical, chemical and

Materials Horizons

COMMUNICATION

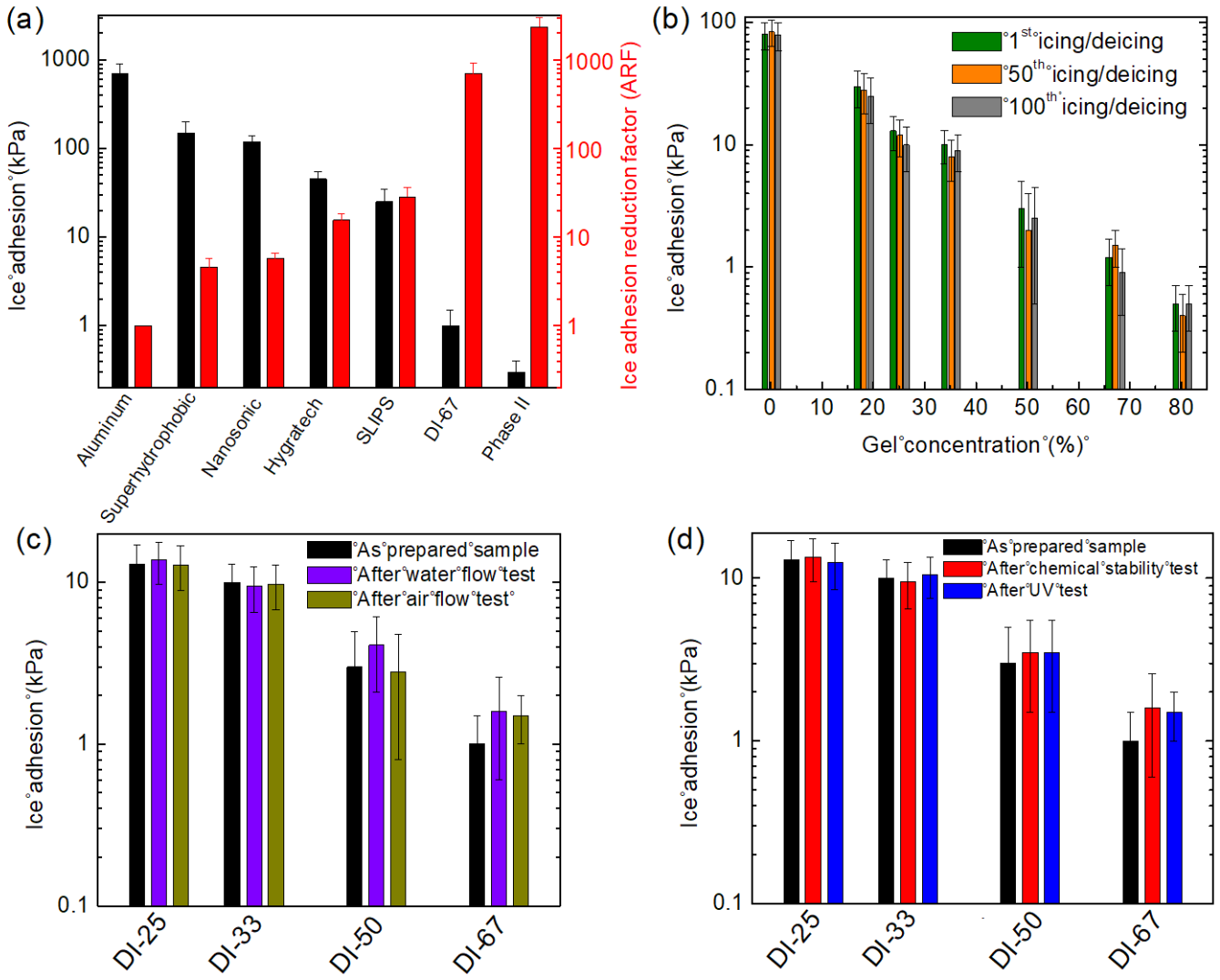

Figure 2. (a) Ice adhesion of state-of-the-art materials is compared with stress-localized icephobic (or de-icing (DI)) coatings. A standard procedure was followed in all the measurements. Furthermore, ice adhesion on pure phase II is reported. In addition, ARF is plotted with the red color. (b) The role of concentration of phase II on ice adhesion is shown. Note that the measured ice adhesion values are independent of icing/deicing cycles. (c) Ice adhesion of the icephobic samples exposed to water and air shear flow with Reynolds number of 2×10^4 and 3×10^4, respectively for one month is shown. (d) Ice adhesion of the icephobic samples exposed to a chemical environment and UV remains unchanged. DI-67, DI-50, DI-33, and DI-25 stand for 67%, 50%, 33%, and 25% of phase II volumetric fraction, respectively.

environmental durability. The icephobic material, stress-localized viscoelastic material, utilizes elastic energy localization at the ice-material interface to shear the interface. With minimal applied force, cracks are formed at the interface generating local stress fields. This shear stress advances cracks at the interface to detach ice form the material. This icephobic (or de-icing (DI)) material is a smooth coating and does not affect the aerodynamic properties of airfoil.

Results

Once ice forms on a surface, the interaction between ice and the substrate is governed by van der Waal's force, electrostatic forces or hydrogen-bonding forces [46,47]. A wide range of surfaces has been studied to reduce ice adhesion strength. Among those, elastomers have shown minimum ice adhesion and have the potential to achieve exceptional icephobic properties [24,38]. Consider a rigid ice phase attached to an elastomer as shown in **Fig. 1a**. If a shear force

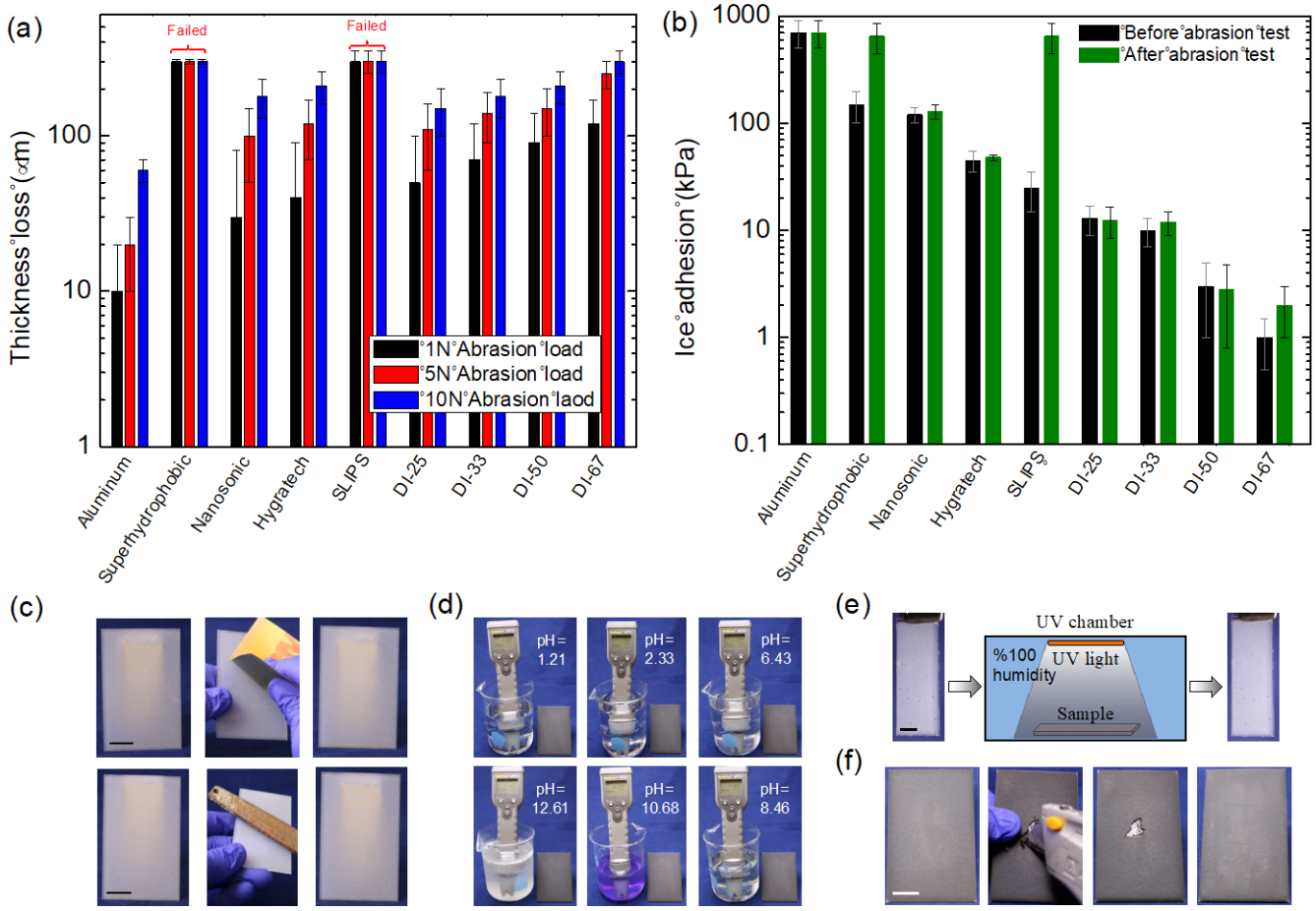

Figure 3. (a) Thickness loss of stress-localized icephobic samples are compared with state-of-the-art technologies (b) Ice adhesion of stress-localized icephobic samples and state-of-the-art technologies before and after 5 N abrasion test. As shown, the new icephobic material keeps low ice adhesion even in highly abrasive environments. Note that sample of pure Phase II is not durable and cannot be tested through abstraction test, **See Supplementary information, S7**. (c) The mechanical durability of stress-localized icephobic material was examined by abrading with sand paper and filing. No change in its properties was measured. (d) The chemical durability of the icephobic coating was examined with a range of chemical solutions with pH in range of 1-13. No change in the integrity of the material was observed. (e) The icephobic material was exposed to UV radiation for 500 hours. No changes to the material's durability were noticed. (f) On-field repairability of the icephobic material is demonstrated by removing some part of the material with a sharp blade and re-spraying of the material. The repaired surface keeps its integrity and icephobic properties. DI-67, DI-50, DI-33, and DI-25 stand for 67%, 50%, 33%, and 25% of phase II volumetric fraction, respectively. Scale bar: 1 cm.

were applied in the ice-elastomer plane, the ice would only slide with no detachment from the surface. However, if the force is applied at a plane higher than the interface, the ice would detach at a critical stress. It has been shown by Chaudhury et al.[48] that the elastic instability at the interface of a rigid body and an elastomer is responsible for fracture. The fingers developed at the contact line by elastic instability elongate and break down in the form of bubbles at the interface. The threshold for bubble formation depends on the shear modulus of the elastomer. For a uniform elastomer with isotropic properties, one finds that the adhesion stress at the interface (σ_s) is written as $\sigma_s \cong \left(\frac{a}{l}\right)\sqrt{\frac{W_a G}{h}}$, where a and l are the geometrical parameters as shown in **Fig. 1a**, W_a is the work of adhesion, G is the shear modulus, and h is the thickness of the elastomer. This formulation suggests that low ice adhesion can be achieved through low values of G and W_a. Note that the value of G can be tuned by several orders of magnitude, but the value of W_a in the best case can be tuned by an order of magnitude (e.g. introduction of perfluorinated groups on a surface). By tuning a material from hard elastomers ($G \sim 1\ GPa$) to gel ($G \sim 1\ Pa$), low values of ice adhesion has been achieved[49]. For example, Beemer et al.[50] used combinations of PDMS formulation to reduce shear modulus and showed consequent decrease in ice adhesion.

However, low values of G lead to low mechanical durability of the icephobic coatings, which results in poor long-term performance. We should add that the values of a, l and h are determined by dimensions of experimental instrument and icephobic material. Inconsistency in these dimensions in measuring of ice adhesion has resulted in scattered data of ice adhesion for the same substrate[40]. We discussed a standard method to measure ice adhesion in the **supplementary information, S1**.

Materials Horizons

COMMUNICATION

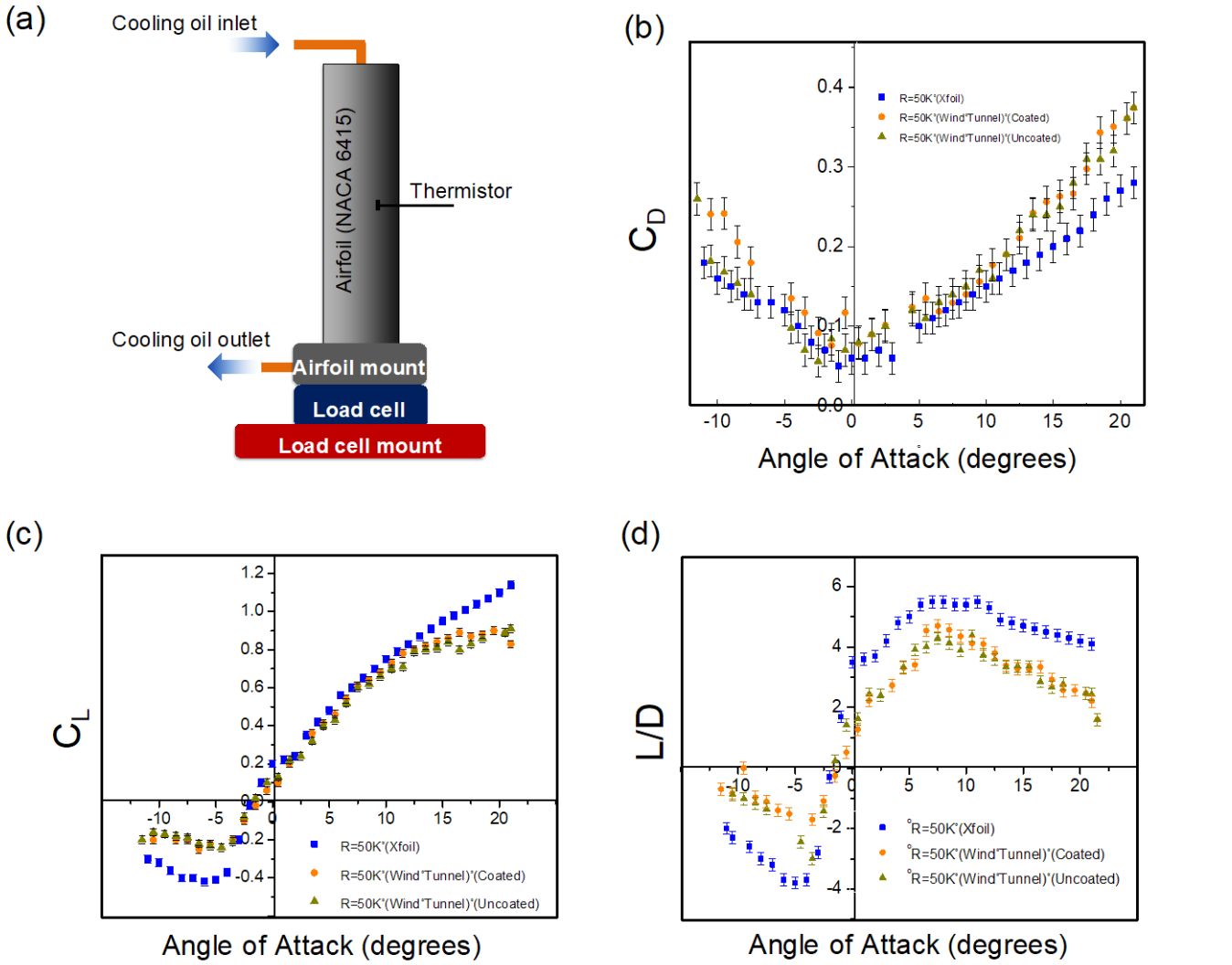

Figure 4. (a) Schematic of experimental set up to determine aerodynamic properties of icephobic coatings, (b) Drag coefficients for both coated and uncoated wings as a function of angle of attack are shown, (c) Lift coefficient remains unchanged with the new icephobic material. (d) Ratio of lift/drag of uncoated and coated airfoil are shown. The results suggest that aerodynamic properties of airfoil remain unchanged with the new coating.

In the above formulation, an isotropic elastomer is considered, which resulted in a direct dependence of σ_s on G. However, once local phases with low shear modulus (i.e. Phase II) are introduced at the ice-material interface, as shown in **Fig. 1b,** with minimal force, ice is detached from phase II and a local cavity (i.e. crack) forms between ice and phase II. This local crack induces an elastic stress field around the crack. This induced shear stress field opens the crack front and leads to propagation of crack at the interface. That is, the induced stress field by local phases leads to crack growth and fracture. Through mathematical formulation of the discussed physics, one finds that the ice adhesion strength on these surfaces is written as (See **supplementary information, S2**)

$$\sigma_s \sim g(\varphi_{\mathrm{II}}) \left(\frac{a}{l}\right) \sqrt{\frac{\overline{W_a}\, G_m}{h}} \qquad (1)$$

Where $g(\varphi_{\mathrm{II}})$ denotes the stress-localization function, φ_{II} is the volumetric fraction of phase II, $\overline{W_a}$ is the work of adhesion of the material, and G_m is the shear modulus of the material. The stress localization function is written as

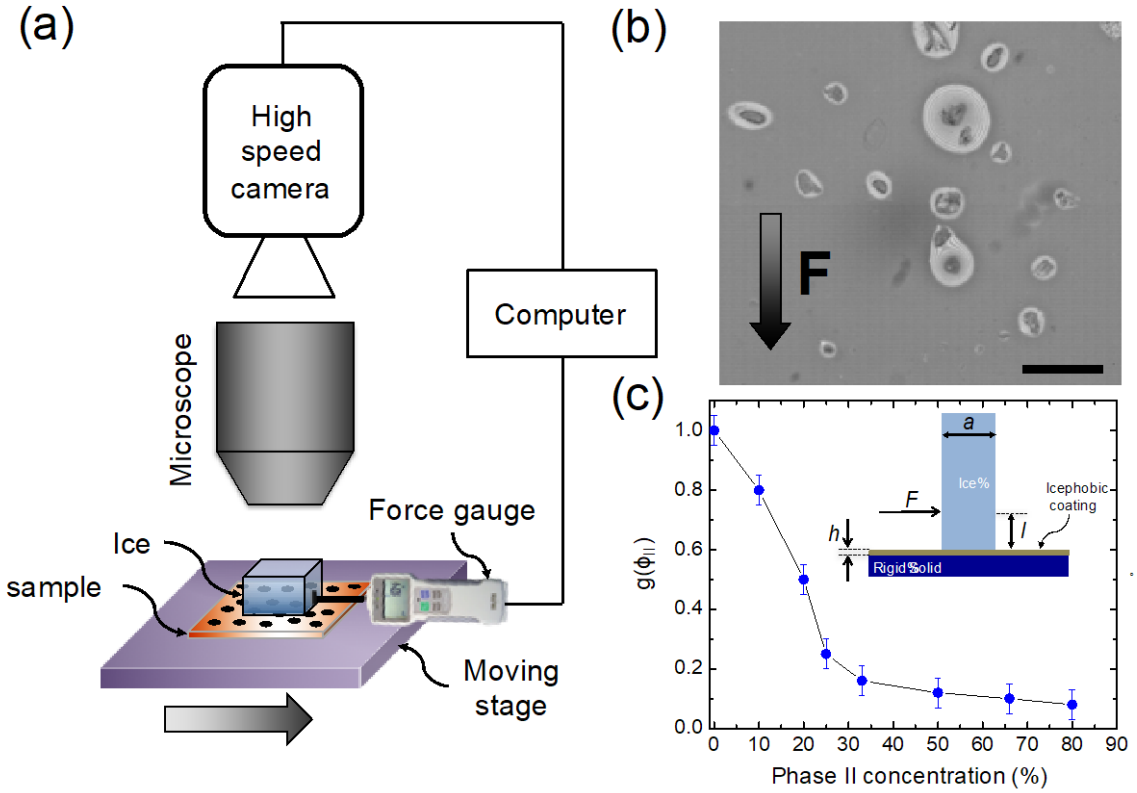

Figure 5. (a) Schematics of the experimental setup to demonstrate crack nucleation between ice and phase II. (b) formation of interfacial cavities observed at coordinate of phase II through coupled optical microscope and high-speed imaging. (c) The stress-localization as a function of concentration of phase II is shown. As shown, stress-localization reduces adhesion of a solid on elastomers up to an order of magnitude. The scale bar is 100 μm.

$$g(\varphi_{\mathrm{II}}) = \frac{1}{\sqrt{\alpha + \beta\, f(\varphi_{\mathrm{II}})\frac{a^2}{l^2}}} \qquad (2)$$

Where $f(\varphi_{\mathrm{II}})$ denotes volumetric fraction of phase II, α is the fraction of contribution of normal stress to the crack growth while β is the fraction of contribution of shear stress to the crack growth (i.e. $\alpha + \beta = 1$). The values of $\overline{W_a}$ and G_m depend on properties of individual phase I and II, their volumetric fraction and their geometry as given in the **supplementary information, S2**. The salient feature of **Eq. 1** is the stress-localization function, which plays a critical role in the adhesion of ice to the material and its impact is far more effective than other parameters studied before (i.e. work of adhesion and shear modulus). This localization function reduces the adhesion of a solid on an elastomer by an order of magnitude as demonstrated and discussed below.

Based on the developed stress-localization concept, we developed a new form of icephobic surface, stress-localized viscoelastic material. The material includes a matrix as phase I with high shear modulus and highly dispersed phase II with low shear modulus. The procedure for development of one form of these materials is given in **supplementary information, S3**. Phase I is a silicon elastomer and phase 2 is a silicon-based organogel. As the matrix of this material plays a major role in long-term mechanical durability, it is crucial to choose an elastomer with high shear modulus. The silicone elastomers in this work are room temperature vulcanizing (RTV) with given mechanical properties in the **supplementary information, S3**. To form a homogenous material, compatibility of the matrix and the dispersed phase is critical. Thus, silicon-based organogel particles with dimension of 2-20 μm were developed as discussed in the **supplementary information, S3**. We measured dimension of organogel particles by analysing them under optical microscope before inclusion in phase I. These dimensions were the minimum size that we could synthesize the gel particles. We should add that dimension of phase II particles affects the localized energy as discussed in Eq. 11 in **supplementary information, S2**. Other combinations of elastomers and the dispersed phases may be used as long as they provide a homogenous material. Once the material is developed, its viscosity could be adjusted through a solvent. Here, we used Hexamethyldisiloxane to reduce the viscosity of the material. In the dilute form, the material could be brushed or sprayed to form a uniform coating. Once applied, the material is completely cured after 24 hrs. A demonstration of this icephobic material is shown in **supplementary video 1**. We examined surface of these materials through Scanning Probe Microscopy (SPM) (Bruker Multimedia 8 SPM) to determine distribution of phase II on the surface. **Fig. 1c** shows modulus of elasticity of both phases. As shown, phase II has a much smaller modulus than that of the matrix. In the next step, we assessed ice adhesion on the developed icephobic material through the discussed standard protocol in **supplementary information, S1**. We developed four types of these materials by tuning the volumetric ratio of phase II in the material. DI-67, DI-50, DI-33, and DI-25 stand for 67%, 50%, 33%, and 25% of phase II, respectively. The measured values of ice adhesion at -25 °C on all these samples are shown in **Fig. 2a**. With the same experimental protocol, we measured ice adhesion on

other state-of-the-art icephobic coatings and included in **Fig. 2a**. The reported value of ice adhesion (σ_s) is the average of ten measurements as followed by the standard protocol, **supplementary information, S4**. We should add that ice adhesion on pure phase I is 80 $\pm$ 25 kPa, while this adhesion for pure phase II is 300 $\pm$ 100 Pa. In the protocol of ice adhesion, the role of material thickness on ice adhesion is discussed. Therefore, all the samples have the same thickness of $300 \pm 20\ \mu m$. As shown, ice adhesion on DI-10 is an order of magnitude lower than other state-of-the-art surfaces. This low ice adhesion is achieved through stress-localization function, $g(\varphi_{\mathrm{II}})$ as discussed below. Another important metric for assessment of ice adhesion on coatings of uniform thickness is ice adhesion reduction factor (ARF) which is defined as $\mathrm{ARF} = \sigma_{\mathrm{s}}\ (\mathrm{Al}) / \sigma_{\mathrm{s}}\ (\mathrm{icephobic\ material})$. This criterion is a non-dimensional figure to determine ice adhesion, independent of geometry of measurement setup. The ARF values for various samples are included in **Fig. 2a** showing that DI-67 reduces ice adhesion by 800 times compared to Aluminium substrate. For some of the state-of-the-art materials, ice adhesion depends on the number of icing/deicing cycles as the properties of these materials (i.e. surface characteristics) changes. For examples, for liquid-infused surfaces, the depletion of liquid on the surface adversely affects cyclic ice adhesion. For the developed stress-localized icephobic surfaces, we determined ice adhesion up to 100 icing/deicing cycles as discussed in the **supplementary information, S5** and no change was observed, **Fig. 2b**. These experiments were conducted for various grades of these stress-localized materials. To assess ice adhesion of these materials in harsh environments, the icephobic coating was exposed to high shear flow of water and air up to Reynolds number of 2×10^4 and 3×10^4, respectively for one month as discussed in the **supplementary information, S6**. With the standard procedure, the ice adhesion was measured after exposure to water and air, **Fig. 2c**. No change in the ice adhesion was observed. To resemble samples exposed to various chemical environments, we exposed the icephobic samples to solutions with pH ranging 1-13 and re-examined the ice adhesion with the standard protocol as presented in **Fig. 2d**. Furthermore, to demonstrate long-term ice adhesion of icephobic samples exposed to UV radiation in the environment, the samples were placed in a UV chamber and kept for 4 weeks. The ice adhesion before and after UV exposure remains unchanged.

We examined mechanical, chemical and environmental durability of the developed icephobic materials. The mechanical durability of the icephobic coatings was examined through Taber abrasion test (Taber Reciprocating Abraser, Model 5900) according to ASTM D4060. In these experiments, material removal at various loading conditions (i.e. 1, 5, and 10 N) was measured. Samples are placed firmly on a horizontal plate in the Taber instrument and 1000 abrasion cycles applied in each experiment. Superhydrophobic surfaces and SLIPS failed all the tests. DI-67 (67 % phase II concentration) failed the 10 N abrasion test. However, other DI samples passed the test in all loading conditions. The thickness removal in the abrasion tests is shown in **Fig. 3a**. Note that the sample of pure phase II is not mechanically durable as shown in **supplementary information, S7.** After abrasion test under 5 N loading for 1000 cycles, the icephobic performance of coatings was re-examined. The ice adhesion for these samples along with state-of-the-art icephobic surfaces are shown in **Fig. 3b**. As shown, no measurable change in ice adhesion was observed and the DI samples offered minimal ice adhesion. In contrast to surface-modified materials (i.e. superhydrophobic surfaces or hydrated-surfaces), the stress-localization property of these materials is volumetric and does not change as they abrade. This feature ensures low ice adhesion on these stress-localized viscoelastic materials for long-term performance. As another metric for its mechanical durability, the icephobic coating was abraded through sand paper and iron file, **Fig. 3c.** The coating holds its low ice adhesion as the icephobic characteristics is a volumetric property and not a surface property.

Depending on the application, the icephobic coatings may be exposed to various chemical environments. The chemical stability of the DI coatings was examined in a range of solutions with pH between 1-13. The acidic solutions were prepared through various HCl and water concentrations. The basic solutions were Tris 0.15 mM NaCl (pH=8) and Sodium hydroxide (pH=13) solutions. The samples were soaked in these solutions for 48 hrs. **Fig. 3d** shows the integrity of the coatings after being exposed to these chemical environments. No change in the ice adhesion of these coatings was detected after chemical stability test. To assess environmental durability of icephobic coatings, the samples were tested for UV radiation effects. The icephobic sample was placed in a chamber for 500 hours under UV radiation. No cracks or material degradation was spotted as shown in **Fig. 3e**. After UV exposure, the icephobic coating was re-examined under abrasive loading of 5 N. The amount of material removed from the coating remained the same as before UV radiation. That is, the integrity of the coating is not affected by UV radiation. Finally, to demonstrate on-field repairability of this coating, the coating is damaged with a sharp blade to remove a part of material. The coating is then repaired by spraying a new coating. The newly sprayed icephobic material is integrated within the coating and no visible change in the coating is observed, **Fig. 3f**.

In aerospace applications, icephobic coatings should have minimal effect on the aerodynamic characteristic of the airfoil (i.e. drag and lift). To examine these characteristics, we chose a wing with a cross section close to NACA 6415 airfoil profile. The experimental setup included two wing sections, which were removed from a small, commercially available wind turbine (ALEKO Vertical Wind Power Generator) in which they were used as the turbine blades to generate torque for a small generator. Of the two wing sections, one was coated with the icephobic material and the other one was left uncoated. The wings were placed in a recirculating wind tunnel with a rectangular test section with a cross-section measuring 1.05 m x 1.65 m. Wing sections were tested at a flow speed of 17 m/s, which corresponds to a chord Reynolds number of approximately 50,000. The details of the experimental procedure are provided in the **supplementary information, S8**. The experimental setup is shown in **Fig. 4a**. The lift and drag coefficients for the coated and uncoated wing sections are plotted against angle of attack in **Fig. 4b and Fig. 4c.** Furthermore, the ratio of lift/drag versus angle of attack is plotted in **Fig. 4d**. The experimental data for both coefficients of lift and drag are accompanied by error bars, which were calculated based on the resolution of the load cell. The XFOIL data do not have any corresponding error bars, since it is a computational value. The results indicate that lift and drag for the coated wing and the uncoated wing have a similar trend for different angles of attack and the difference in magnitudes on both is small. The magnitude of lift and drag coefficients of the airfoil found experimentally differs from the XFOIL computational results because XFOIL is a 2D computational tool that does not account for three-dimensional effects, such as the 3D characteristics of the finite wing. In a finite wing, the higher-pressure air from beneath the wing tries to move towards the lower pressure above the wing. Moreover, the new experimental data indicate that the coating

does not affect the lift and drag characteristics of a wing, which is important in any passive anti-icing aerospace systems.

To demonstrate the role of stress localization function, $g(\varphi_{\mathrm{II}})$, on the ice adhesion, we designed an experimental procedure to probe crack nucleation at the material-ice interface. A form of the icephobic material is developed and was applied to a glass substrate. The coating includes PDMS matrix and black organogel particles to provide contrast for visualization of crack nucleation at the material-ice interface. A silanized glass prism (15 mm × 15 mm × 25 mm) was placed on the icephobic material to resemble interaction of ice with the coating. The glass substrate was placed on a moving stage, the movement of which is controlled by a motorized motion controller and computer. The motorized stage is a syringe pump with forward velocity variation of 0.5 µm/s to 5 mm/s. A firmly held beam load cell (Imada, model DS2-110) is used to measure the force. The force was applied at a distance of 1 mm above the interface. The interface of the icephobic material-prism was viewed as shown in **Fig. 5a**. Through a coupled optical microscope and a high-speed camera system, the crack nucleation at the interface was probed. **Figure 5b** shows micrograph of interfacial cracks observed during these experiments. As shown, all the interfacial cracks are formed at the coordinate of phase II. That is, phase II is responsible for cavitation and crack initiation at the interface. The fringes observed at the crack coordinates indicate the ellipsoidal form of these cavities. The generated crack induces local stress field and the stored elastic energy depends on shear modulus of phase I and the dimension of these cracks. (i.e. $U_L \propto G\, r^3$). This stored elastic energy leads to a shear force at perimeter of crack, propagation of crack, and detachment of ice from the material. The mathematical derivation of this physics is discussed in **supplementary information, S2**.

To determine the value of stress-localization function, $g(\varphi_{\mathrm{II}})$, for the stress-localized icephobic materials, we determined the values of G_m and $\overline{W_a}$ of the developed icephobic materials as discussed in the **supplementary information, S9**. These values are tabulated in **Table S3 in the supplementary information**. Given the measured ice adhesion on these surfaces, **Fig. 2a**, dimension of experimental setup and the measured properties in Table S3, we obtained the values of $g(\varphi_{\mathrm{II}})$ through **Eq. 1** and plotted in **Fig. 5c**. As shown, the stress localization function depends on the concentration of phase II in the material structure as predicted. This stress-localization function reduces ice adhesion on the icephobic material up to an order of magnitude. We should emphasize that the role of $g(\varphi_{\mathrm{II}})$ on reduction of ice adhesion is several times higher than the role of shear modulus, G_m. For example, comparing the sample DI-67 (σ_s= 1-2 kPa) and pure silicon elastomer (σ_s= 80 kPa), the difference of shear modulus is approximately six times which results in ~ 2.5 times reduction in ice adhesion. However, for the same samples, stress localization reduces the ice adhesion by more than 12 times. For coatings with high concentration of phase II**,** ice easily detaches from phase II (low shear modulus) which forms major part of the interface. As detachment of ice from phase II is governed by normal stress, value of α increases while value of β decreases. Thus, $g(\varphi_{\mathrm{II}})$ increases. The developed theory covers all range of concentrations. However, for high concentration of phase II, the coatings are not durable and functional. Thus, we did not include them in our work.

Note that stress-localization function could be determined through first-principles if fracture mechanism is known. In **Eq. 2,** the values of α and β are determined through knowledge on fracture mechanism and depend on the interaction of solid and the coating. For example, for uniform elastomers, normal stress is responsible for crack growth resulting in α of unity and β of zero and consequently $g(\varphi_{\mathrm{II}}) = 1$. For very thin solid material on a surface (e.g. bio-films), the contribution of normal force goes to zero ($\alpha = 0$) and the crack growth is dominated by shear stress ($\beta = 1$). Note that as $a/l \gg 1$, stress-localization function is always $0 < g(\varphi_{\mathrm{II}}) \leq 1$. As an estimate, we determined value of stress-localization function for icephobic surfaces with 10% and 20% concentration of phase II and considering $\alpha = \beta = 0.5$. This results in $g(\varphi_{\mathrm{II}})$ of 0.76 and 0.58 while the measured values of $g(\varphi_{\mathrm{II}})$ are 0.8 ± 0.05 and 0.5 ± 0.05, respectively suggesting a close agreement. The stress localization function also depends on geometrical parameters (a and l). For low values of a/l the role of normal force is dominant in the fracture and the role of stress localization (i.e. shear force) is small. However, for high values of a/l, the fracture is governed by shear forces and the stress localization is the dominant factor. The developed physic of stress-localization is applicable in detachment of any solid material (ice, dust and even bio-species) from elastomers.

Conclusions

In summary, we report a new physical concept and corresponding material paradigm to develop highly durable icephobic materials. These materials utilize stress-localization function to induce crack at the ice-material interface and consequently minimize ice adhesion on the material. Stress-localization leads to a shear force at the interface for detachment of ice from the material. The developed concept is implemented in elastomers and the superior icephobicity of these materials compared to state-of-the-art materials is demonstrated. This form of icephobic materials demonstrates excellent mechanical, chemical and environmental durability with no change in characteristics under extreme air and water shear flows. Furthermore, these icephobic materials do not change the aerodynamic characteristics of airfoil thereby providing a promising solution for aerospace applications. In contrast to surface-modified coatings, the icephobicity of these materials is a volumetric property and no degradation in the performance occurs in long-term operation under mechanical loadings. The developed concept of stress-localization reduces adhesion of solids on a material by an order of magnitude with no compromise in mechanical properties. We envision that the developed physical concept opens a rational route to minimize adhesion of any solid species (i.e. ice, gas hydrate, dust, and even bio-species) on a surface with omnipresent application in transportation systems (aviation, cars and vessels), energy systems, and biotechnologies.

Author contributions

H. G. and P. I. conceived the research. P. I. developed the experimental setups. P. I., A. B, and B. E. conducted the icephobicity experiments. T. S. and D. A. conducted the aerodynamics experiments. P. I., M. N., P. J., V. K., and A. M. conducted durability experiments. H. G. conducted the theoretical analysis. P. I. and H. G. wrote the manuscript.

Conflicts of interest

There are no conflicts to declare.

Acknowledgments

H. G. acknowledges funding support from National Science Foundation (Grant NSF- 1804204) with Dr. Susan Muller as program

manager and Air Force Office of Scientific Research (Grant AFOSR FA9550-16-1-0248) with Dr. Ali Sayir as program manager.

References

(1) Jia, Z.; DeLuca, C. I.; Chao, H.; Davies, P. L. *Nature* **1996**, *384*, 285–288.
(2) Liou, Y. C.; Tocilj, a; Davies, P. L.; Jia, Z. *Nature* **2000**, *406*, 322–324.
(3) Dalili, N.; Edrisy, A.; Carriveau, R. *Renew. Sustain. Energy Rev.* **2009**, *13*, 428–438.
(4) Andersson, A. K.; Chapman, L. *Accid. Anal. Prev.* **2011**, *43*, 284–289.
(5) Gent, R. W.; Dart, N. P.; Cansdale, J. T. *Phil. Trans. R. Soc. Lond.* **2000**, *358*, 2873–2911.
(6) Marwitz, J.; Politovich, M.; Bernstein, B.; Ralph, F.; Neiman, P.; Ashenden, R.; Bresch, J. *Bull. Am. Meteorol. Soc.* **1997**, *78*, 41–52.
(7) Laforte, J. L.; Allaire, M. a.; Laflamme, J. *Atmos. Res.* **1998**, *46*, 143–158.
(8) Arctic Council. *Arctic Marine Infrastructure*; 2009.
(9) Jiang, X.; Zhao, J.; Luo, B.; Zhang, J.; Huang, C. In *IWAIS XIII*; Andermatt, Switzerland, 2009.
(10) Antonini, C.; Innocenti, M.; Horn, T.; Marengo, M.; Amirfazli, A. *Cold Reg. Sci. Technol.* **2011**, *67*, 58–67.
(11) Campbell, R. J. *Congr. Res. Serv. Rep.* **2012**, 1–15.
(12) LaCommare, K. H.; Eto, J. H. *Cost of Power Interruptions to Electricity Consumers in the United States (U.S.)*; 2006.
(13) Lafuma, A.; Quéré, D. *Nat. Mater.* **2003**, *2*, 457–460.
(14) Deng, X.; Mammen, L.; Butt, H. J.; Vollmer, D. *Science (80-.).* **2012**, *335*, 67–70.
(15) Zhang, Q.; He, M.; Chen, J.; Wang, J.; Song, Y.; Jiang, L. *Chem. Commun.* **2013**, *49*, 4516–4518.
(16) Kulinich, S. A.; Farhadi, S.; Nose, K.; Du, X. W. *Langmuir* **2011**, *27*, 25–29.
(17) Nosonovsky, M.; Hejazi, V. *ACS Nano* **2012**, *6*, 8488–8491.
(18) Chavan, S.; Carpenter, J.; Nallapaneni, M.; Chen, J. Y.; Miljkovic, N. *Appl. Phys. Lett.* **2017**, *110*.
(19) Sojoudi, H.; Wang, M.; Boscher, N. D.; McKinley, G. H.; Gleason, K. K. *Soft Matter* **2016**, *12*, 1938–1963.
(20) Herminghaus, S. *Eur. Lett.* **2000**, *52*, 165–170.
(21) Cheng, Y. T.; Rodak, D. E. *Appl. Phys. Lett.* **2005**, *86*, 1–3.
(22) Maitra, T.; Tiwari, M. K.; Antonini, C.; Schoch, P.; Jung, S.; Eberle, P.; Poulikakos, D. *Nano Lett.* **2014**, *14*, 172–182.
(23) Hejazi, V.; Sobolev, K.; Nosonovsky, M. *Sci. Rep.* **2013**, *3*, 2194.
(24) Meuler, A. J.; Smith, J. D.; Varanasi, K. K.; Mabry, J. M.; McKinley, G. H.; Cohen, R. E. *ACS Appl. Mater. Interfaces* **2010**, *2*, 3100–3110.
(25) Chen, J.; Liu, J.; He, M.; Li, K.; Cui, D.; Zhang, Q.; Zeng, X.; Zhang, Y.; Wang, J.; Song, Y. *Appl. Phys. Lett.* **2012**, *101*, 2010–2013.
(26) Wong, T.-S.; Kang, S. H.; Tang, S. K. Y.; Smythe, E. J.; Hatton, B. D.; Grinthal, A.; Aizenberg, J. *Nature* **2011**, *477*, 443–447.
(27) Wilson, P. W.; Lu, W.; Xu, H.; Kim, P.; Kreder, M. J.; Alvarenga, J.; Aizenberg, J. *Phys. Chem. Chem. Phys.* **2013**, *15*, 581–585.
(28) Kreder, M. J.; Alvarenga, J.; Kim, P.; Aizenberg, J. *Nat. Rev. Mater.* **2016**, *1*, 15003.
(29) Rykaczewski, K.; Anand, S.; Subramanyam, S. B.; Varanasi, K. K. *Langmuir* **2013**, *29*, 5230–5238.
(30) Fletcher, N. H. *Philos. Mag.* **1962**, *7*, 255–269.
(31) Fletcher, N. H. *Philos. Mag.* **1968**, *18*, 1287–1300.
(32) Ryzhkin, I.; Petrenko, V. *Phys. Rev. B* **2001**, *65*, 1–4.
(33) Jellinek, H. H. . *J. Colloid Interface Sci.* **1967**, *25*, 192–205.
(34) Rosenberg, R. *Phys. Today* **2005**, *December*, 50–55.
(35) Chen, J.; Dou, R.; Cui, D.; Zhang, Q.; Zhang, Y.; Xu, F.; Zhou, X.; Wang, J.; Song, Y.; Jiang, L. *ACS Appl. Mater. Interfaces* **2013**, *5*, 4026–4030.
(36) Dou, R.; Chen, J.; Zhang, Y.; Wang, X.; Cui, D.; Song, Y.; Jiang, L.; Wang, J. *ACS Appl. Mater. Interfaces* **2014**, *6*, 6998–7003.
(37) Chen, J.; Luo, Z.; Fan, Q.; Lv, J.; Wang, J. *Small* **2014**, *10*, 4693–4699.
(38) Chen, D.; Gelenter, M. D.; Hong, M.; Cohen, R. E.; McKinley, G. H. *ACS Appl. Mater. Interfaces* **2017**, *9*, 4202–4214.
(39) Golovin, K.; Kobaku, S. P. R.; Lee, D. H.; DiLoreto, E. T.; Mabry, J. M.; Tuteja, A. *Sci. Adv.* **2016**, *2*, 1–12.
(40) Wang, C.; Fuller, T.; Zhang, W.; Wynne, K. J. *Langmuir* **2014**, *30*, 12819–12826.
(41) Susoff, M.; Siegmann, K.; Pfaffenroth, C.; Hirayama, M. *Appl. Surf. Sci.* **2013**, *282*, 870–879.
(42) He, Z.; Xiao, S.; Gao, H.; He, J.; Zhang, Z. *Soft Matter* **2017**, *13*, 6562–6568.
(43) Irajizad, P.; Hasnain, M.; Farokhnia, N.; Sajadi, S. M.; Ghasemi, H. *Nat. Commun.* **2016**, *7*, 13395.
(44) Irajizad, P.; Ray, S.; Farokhnia, N.; Hasnain, M.; Baldelli, S.; Ghasemi, H. *Adv. Mater. Interfaces* **2017**, *4*, 1700009.
(45) Masoudi, A.; Irajizad, P.; Farokhnia, N.; Kashyap, V.; Ghasemi, H. *ACS Appl. Mater. Interfaces* **2017**, *9*.
(46) Ryzhkin, I. A.; Petrenko, V. F. *J. Phys. Chem. B* **1997**, *101*, 6267–6270.
(47) Wilen, L. A.; Wettlaufer, J. S.; Elbaum, M.; Schick, M. *Phys. Rev. B* **1995**, *52*, 12426–12433.
(48) Chaudhury, M. K.; Kim, K. H. *Eur. Phys. J. E* **2007**, *23*, 175–183.
(49) Urata, C.; Dunderdale, G. J.; England, M. W.; Hozumi, A. *J. Mater. Chem. A* **2015**, *3*, 12626–12630.
(50) Beemer, D. L.; Wang, W.; Kota, A. K. *J. Mater. Chem. A* **2016**, *4*, 18253–18258.